Available online at www.sciencedirect.com
SCIENCE DIRECT®
International Journal of Thermal Sciences 44 (2005) 513–520
International Journal of Thermal Sciences
www.elsevier.com/locate/ijts

Prediction of heat transfer characteristics in rectangular microchannels for slip flow regime and H1 boundary condition

Lotfollah Ghodoossi [a,*], Nilüfer Eğrican [b]

[a] *Istanbul Technical University, Mechanical Engineering Department, 80191 Gumussuyu, Istanbul, Turkey*
[b] *Yeditepe University, School of Engineering and Architecture, Department of Mechanical Engineering, 26 Agustos Yerlesimi, Kayisdagi Caddesi, 81120 Kayisdagi/Istanbul, Turkey*

Received 7 June 2004; received in revised form 28 November 2004; accepted 24 January 2005

Abstract

Convective heat transfer in a rectangular microchannel under slip flow and H1 boundary condition is studied. Integral transform method is applied to derive the velocity and temperature distributions and thus the average Nusselt number. It is found that rarefaction has a decreasing effect on heat transfer for most engineering microchannel applications, with any aspect ratios. However, an increase in heat transfer with rarefaction is investigated when the influence of temperature jump on solid boundaries is weak. It is also found that the effect of wall temperature on the heat transfer is negligible. The results of paper for the special case of non-slip flow coincide with the results of previous studies.

Keywords: Slip flow; Microchannel; Convection; Heat transfer

1. Introduction

The need for high heat fluxes in small electronic and other devices has caused the microscale heat transfer to be the subject of studies in the past few years. As of today, more studies and attention are required to develop the microscale heat transfer field. As the size of devices falls in the order of a few 100 microns, the physics of fluid flow and heat transfer in such devices changes substantially. Slip flow is an example of such change in the physics of the microscale fluid flow and heat transfer problems.

A gaseous flow at low pressure or in a very small passage does not obey the classical continuum physics. Contrary to the fluid flow in continuum physics, such a flow exhibits a nonzero flow velocity at solid boundaries and a nonzero difference between temperatures of solid boundaries and flow near solid boundaries. In other words, a slip flow and a temperature jump (non-equilibrium thermodynamics) will be present at solid boundaries, which are major effects of rarefaction and change in the physics of flow.

The slip flow problem in microtubes has been widely conducted by investigators [1–8]. However, slip flow in microchannels has not been conducted as much as the slip flow in microtubes. Since the slip flow in microchannels requires a two-dimensional approach, its solution is relatively difficult compared to that of the slip flow in microtubes. Some of the slip flow studies in microchannels are summarized here. Yu and Ameel [9] studied slip flow heat transfer in microchannels and found that heat transfer increases, decreases, or remains unchanged, compared to non-slip flow conditions, depending on two dimensionless variables that include effects of rarefaction and the fluid/wall interaction. Kavehpour et al. [10] have conducted the effects of compressibility and rarefaction in microchannel heat transfer under slip flow. They found that compressibility and rarefaction become important on microchannel heat transfer under slip flow for high and low Reynolds numbers, respectively.

* Corresponding author. Tel.: +90-212-2931300 (2452), fax: +90-212-2450795.
E-mail addresses: kuddusi@itu.edu.tr (L. Ghodoossi), egrican@yeditepe.edu.tr (N. Eğrican).

1290-0729/$ – see front matter
doi:10.1016/j.ijthermalsci.2005.01.006

Nomenclature

a	long side of microchannel
A_n	constant defined by Eq. (37)
b	short side of microchannel
B_n	constant defined by Eq. (38)
c_P	Specific heat
C_n	constant defined by Eq. (49)
C'_n	constant defined by Eq. (50)
D_h	hydraulic diameter
D_n	constant defined by Eq. (54)
F_t	thermal accommodation coefficient
F_v	tangential momentum accommodation coefficient
k	thermal conductivity
K	kernel
Kn	Knudsen number
Nu	Nusselt number
p	fluid pressure
P	normalized pressure gradient
Pr	Prandtl number
q'	thermal power per unit length of microchannel
R	specific heat ratio
S_1, S_2, S_3, S_4	constants introduced for simplicity
T	temperature
$\widehat{T}$	nondimensional temperature
u	fluid velocity
$\widehat{u}$	nondimensional fluid velocity
v	dependent variable defined by Eq. (20)
x, y, z	nondimensional coordinates

Greek symbols

α	thermal diffusivity
β	nondimensional variable defined by Eq. (58)
β_t	nondimensional variable defined by Eq. (3)
β_v	nondimensional variable defined by Eq. (4)
γ	aspect ratio
λ_{mfp}	molecular mean free path
μ	eigenvalues
ρ	density
θ	dependent variable defined by Eq. (21)
$\bar{\theta}$	transformed dependent variable defined by Eq. (46)
ξ, η, ζ	coordinates

Subscripts

b	bulk property
m	mean value
n	index
s	fluid property near the wall
w	wall value
0	inlet property

Vasudeviah and Balamurugan [11] studied incompressible convective heat transfer in a microchannel with respect to rarefied gas flows and found analytical expressions for the mean Nusselt number. Tunc and Bayazitoglu [12] studied microchannel heat transfer under slip flow and H2 boundary condition (constant axial and peripheral heat flux) and found that increasing the rarefaction shows a decreasing effect on the heat transfer.

The purpose of this paper is to find the temperature distribution and thus the mean Nusselt number in a microchannel under slip flow and H1 boundary condition (constant axial heat flux and uniform peripheral wall temperature). The integral transform method is applied to solve the momentum and energy equations. An explicit expression is found for the mean Nusselt number, which is a function of the aspect ratio, the wall temperature and the rarefaction including the effects of thermal and momentum accommodation factors.

The results of the paper for the special case of non-slip flow ($Kn = 0$) coincide with the results of Morini [13] who solved the non-slip flow in ducts under H1 boundary condition. The numerical values of Nusselt number found in this paper are also in good agreement with the numerical values of the "developed" Nusselt number found by Yu and Ameel [9].

2. Problem statement

Consider a hydrodynamically and thermally developed steady flow in a rectangular microchannel. If the flow pressure is low, or, the microchannel sizes are very small, which is supposed to be the case in this paper, a slip flow occurs. Different from non-slip flow, the flow velocity is no longer zero at microchannel walls under slip flow. A molecular flow with nonzero velocity at microchannel boundaries occurs. Apart from nonzero flow velocity at the boundaries, a nonzero difference between the temperatures of the boundaries and the flow near the boundaries occurs as well. The effect of rarefaction on flow properties is quantified by introducing the Knudsen number, which is defined as the ratio of the mean free molecular path to the characteristic length of flow field. The Knudsen number equal to zero corresponds to non-slip flow with zero flow velocity and zero difference between the temperatures of the boundaries and adjacent flow. As the Knudsen number takes a nonzero value, a slip flow with nonzero flow velocity at the boundaries and nonzero temperature difference between the boundaries and adjacent flow takes place. The higher Knudsen number causes higher rarefaction effects, namely, higher flow velocity and temperature jump at the boundaries. Beskok and Karniadakis [14] give the classification to differentiate the flow

types. In this paper the concentration is on the slip flow with $10^{-3} \leqslant Kn < 10^{-1}$.

The flow is governed by the Navier–Stokes equations if the continuum condition (very low Knudsen number, $Kn < 10^{-3}$) is satisfied. The continuum form of flow does not exist in a microchannel under slip flow. Therefore the slip flow solution by using the Navier–Stokes equations may result in no negligible deviations in the hydrodynamic and thermal properties of the flow. However, the general belief of the investigators is that the Navier–Stokes equations may be used for slip flow solution with high accuracy provided the boundary conditions are modified according to the slip flow characteristics. Modification of the boundary conditions (nonzero flow velocity and temperature jump at the boundaries) removes the error raised by not properly using the Navier–Stokes equations in slip flow solution. The procedure is explained in the following sections.

3. Governing equations and modified boundary conditions

The geometry of the microchannel is shown in Fig. 1. The H1 boundary condition implies that the wall temperature T_w is uniform along perimeter at a specified ζ-cross section of microchannel and it increases linearly with ζ. The H1 boundary condition will be matched with slip flow properties to determine the modified boundary conditions.

If the problem under consideration was a non-slip flow, the temperature of the flow near the wall would be equal to the wall temperature T_w and the velocity of the flow near the wall would be equal to zero. Since the problem under consideration is a slip flow, the temperature of the flow near the wall is no longer equal to the wall temperature and the velocity of the flow near the wall is no longer zero. The local temperature and velocity of the flow near the bottom wall are given by Barron et al. [1], as

$$T_s(\xi) = T_w + \beta_t \lambda_{\mathrm{mfp}} \frac{\partial T}{\partial \eta}\Big|_{\eta=0} \tag{1}$$

$$u_s(\xi) = \beta_v \lambda_{\mathrm{mfp}} \frac{\partial u}{\partial \eta}\Big|_{\eta=0} \tag{2}$$

where

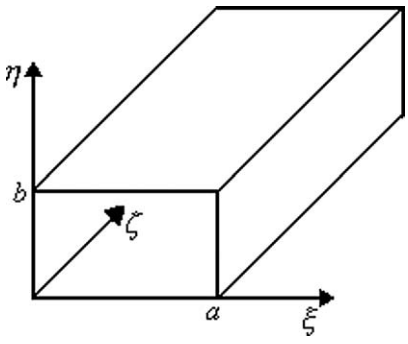

Fig. 1. The geometry of microchannel.

$$\beta_t = \frac{2 - F_t}{F_t} \frac{2R}{1+R} \frac{1}{Pr} \tag{3}$$

$$\beta_v = \frac{2 - F_v}{F_v} \tag{4}$$

The parameters F_t and F_v are thermal accommodation coefficient and tangential momentum accommodation coefficient, respectively. For real walls some molecules reflect diffusively and some reflect specularly. These coefficients are defined as the fraction of molecules reflected diffusively [15]. Depending on the fluid, the solid and the surface finish these coefficients vary from 0 to 1.

Eqs. (1) and (2) will guide us to set the modified thermal and hydrodynamic boundary conditions of the flow at the walls. The local temperature and velocity of the flow near the walls will be integrated along the walls and averaged over the perimeter to set the thermal (T_s) and hydrodynamic (u_s) boundary conditions at the walls, respectively.

The governing Navier–Stokes equations (ζ-direction momentum and energy equations) for a hydrodynamically and thermally developed flow are

$$\frac{\partial^2 u}{\partial \xi^2} + \frac{\partial^2 u}{\partial \eta^2} = \frac{1}{\mu} \frac{\partial p}{\partial \zeta} \tag{5}$$

$$\frac{\partial^2 T}{\partial \xi^2} + \frac{\partial^2 T}{\partial \eta^2} = \frac{u(\xi,\eta)}{\alpha} \frac{\partial T}{\partial \zeta} \tag{6}$$

The modified hydrodynamic and H1 thermal boundary conditions according to the slip flow assumption are

$$u = u_s \quad \text{at } \xi = 0,\ \xi = a,\ \eta = 0, \eta = b \tag{7}$$

$$T = T_s \quad \text{at } \xi = 0,\ \xi = a,\ \eta = 0,\ \eta = b \tag{8}$$

The axial variation of fluid temperature is approximated in the following form by providing an energy balance for an arbitrary differential $\mathrm{d}\zeta$ segment of the microchannel

$$\frac{\partial T}{\partial \zeta} = \frac{q'}{\rho c_P u_m ab} \tag{9}$$

where u_m represents the mean fluid velocity, which is defined as

$$u_m = \frac{1}{ab} \int_0^b \int_0^a u(\xi,\eta)\, \mathrm{d}\xi\, \mathrm{d}\eta \tag{10}$$

The momentum and energy equations and the modified boundary conditions are nondimensionalized by introducing the following nondimensional variables.

$$x = \frac{\xi}{a}, \quad 0 \leqslant x \leqslant 1 \tag{11}$$

$$y = \frac{\eta}{a}, \quad 0 \leqslant y \leqslant \gamma \equiv \frac{b}{a} \tag{12}$$

$$\widehat{u}(x,y) = \frac{u(\xi,\eta)}{u_m} \tag{13}$$

$$\widehat{T} = \frac{T - T_0}{(q'/k)} \tag{14}$$

The nondimensional momentum and energy equations and associated boundary conditions are found as

$$\frac{\partial^2 \widehat{u}}{\partial x^2} + \frac{\partial^2 \widehat{u}}{\partial y^2} = P \tag{15}$$

$$\frac{\partial^2 \widehat{T}}{\partial x^2} + \frac{\partial^2 \widehat{T}}{\partial y^2} = \frac{1}{\gamma}\widehat{u}(x, y) \tag{16}$$

$$\widehat{u} = \widehat{u}_s \quad \text{at } x = 0,\ x = 1,\ y = 0,\ y = \gamma \tag{17}$$

$$\widehat{T} = \widehat{T}_s \quad \text{at } x = 0,\ x = 1,\ y = 0,\ y = \gamma \tag{18}$$

where the normalized pressure gradient P is defined as

$$P = \frac{a^2}{u_m \mu}\frac{\partial p}{\partial \zeta} \tag{19}$$

Each of the nondimensional momentum and energy equations contain four nonhomogeneous boundary conditions. The nonhomogeneous boundary conditions of the nondimensional momentum and energy equations in y-direction are homogenized by means of change of dependent variables defined, respectively, as

$$v(x, y) = \widehat{u}(x, y) - \widehat{u}_y(y) \tag{20}$$

$$\theta(x, y) = \widehat{T}(x, y) - \widehat{T}_y(y) \tag{21}$$

where the auxiliary one direction $\widehat{u}_y(y)$ and $\widehat{T}_y(y)$ functions satisfy the following differential equations and the same boundary conditions for the nondimensional momentum and energy equations at $y = 0$ and$y = \gamma$, respectively.

$$\frac{\mathrm{d}^2 \widehat{u}_y}{\mathrm{d}y^2} - \widehat{u}_y = 0 \tag{22}$$

$$\frac{\mathrm{d}^2 \widehat{T}_y}{\mathrm{d}y^2} - \widehat{T}_y = 0 \tag{23}$$

$$\widehat{u}_y = \widehat{u}_s \quad \text{at } y = 0,\ y = \gamma \tag{24}$$

$$\widehat{T}_y = \widehat{T}_s \quad \text{at } y = 0,\ y = \gamma \tag{25}$$

The solutions of system above are found as

$$\widehat{u}_y = \frac{\widehat{u}_s}{1 + e^{\gamma}}\left(e^{y} + e^{\gamma - y}\right) \tag{26}$$

$$\widehat{T}_y = \frac{\widehat{T}_s}{1 + e^{\gamma}}\left(e^{y} + e^{\gamma - y}\right) \tag{27}$$

By applying the change of dependent variables as defined above the governing nondimensional momentum and energy equations and associated boundary conditions take the following form, respectively.

$$\frac{\partial^2 v}{\partial x^2} + \frac{\partial^2 v}{\partial y^2} = P - \frac{\widehat{u}_s}{1 + e^{\gamma}}\left(e^{y} + e^{\gamma - y}\right) \tag{28}$$

$$v = \widehat{u}_s - \widehat{u}_y \quad \text{at } x = 0,\ x = 1 \tag{29}$$

$$v = 0 \quad \text{at } y = 0,\ y = \gamma \tag{30}$$

$$\frac{\partial^2 \theta}{\partial x^2} + \frac{\partial^2 \theta}{\partial y^2} = \frac{1}{\gamma}\widehat{u}(x, y) - \frac{\widehat{T}_s}{1 + e^{\gamma}}\left(e^{y} + e^{\gamma - y}\right) \tag{31}$$

$$\theta = \widehat{T}_s - \widehat{T}_y \quad \text{at } x = 0,\ x = 1 \tag{32}$$

$$\theta = 0 \quad \text{at } y = 0,\ y = \gamma \tag{33}$$

The system above will be solved in two steps. First, the momentum equation (Eqs. (28)–(30)) will be solved to determine the velocity distribution. The velocity distribution will be used to solve the energy equation (Eqs. (31)–(33)) in the next step. Integral transform method is applied to solve both the momentum and energy equations.

4. Solution of the momentum and energy equations

The momentum equation in slip flow is already solved by Tunc and Bayazitoglu [12]. Applying a similar procedure gives the velocity distribution as

$$\widehat{u}(x, y) = \frac{\widehat{u}_s}{1 + e^{\gamma}}\left(e^{y} + e^{\gamma - y}\right) + \sum_{n=1}^{\infty} K(\mu_n, y) \times \left\{\frac{B_n[\sinh \mu_n x - \sinh \mu_n (x - 1)]}{\sinh \mu_n} - \frac{A_n}{\mu_n^2}\right\} \tag{34}$$

where

$$K(\mu_n, y) = \sqrt{\frac{2}{\gamma}}\sin \mu_n y \tag{35}$$

$$\sin \mu_n \gamma = 0,\ \text{or},\ \mu_n = \frac{n\pi}{\gamma}, \quad n = 1, 2, 3, \ldots \tag{36}$$

$$A_n = \left[-(-1)^n + 1\right]\sqrt{\frac{2}{\gamma}}\frac{1}{\mu_n}\left(P - \frac{\widehat{u}_s \mu_n^2}{1 + \mu_n^2}\right) \tag{37}$$

$$B_n = \sqrt{\frac{2}{\gamma}}\frac{P[-(-1)^n + 1]}{\mu_n^3} \tag{38}$$

$$P = \frac{1}{8S_1}\left\{\gamma^2 - \widehat{u}_s\left[\frac{2(e^{\gamma} - 1)\gamma}{1 + e^{\gamma}} + 8S_2\right]\right\} \tag{39}$$

$$\widehat{u}_s = \frac{S_3}{S_1}\frac{\gamma}{2\left[\frac{1+\gamma}{2\gamma\beta_v Kn} - \frac{1-e^{\gamma}}{1+e^{\gamma}}\left(1 + \frac{S_3}{S_1}\right) - \frac{4}{\gamma}S_2\left(\frac{S_4}{S_2} - \frac{S_3}{S_1}\right)\right]} \tag{40}$$

$$S_1 = \sum_{n=1}^{\infty}\frac{2\tanh \mu_{2n-1}/2 - \mu_{2n-1}}{\mu_{2n-1}^5} \tag{41}$$

$$S_2 = \sum_{n=1}^{\infty}\frac{1}{\mu_{2n-1}^2(1 + \mu_{2n-1}^2)} \tag{42}$$

$$S_3 = \sum_{n=1}^{\infty}\frac{2\tanh \mu_{2n-1}/2 - \mu_{2n-1}}{\mu_{2n-1}^3} \tag{43}$$

$$S_4 = \sum_{n=1}^{\infty}\frac{1}{1 + \mu_{2n-1}^2} \tag{44}$$

$$Kn = \frac{\lambda_{\mathrm{mfp}}}{D_h} \tag{45}$$

The integral transform and inversion formula to be used in solution of the energy equation are

Integral transform

$$\bar{\theta}(\mu_n, x) = \int_0^{\gamma} K(\mu_n, y)\theta(x, y)\,\mathrm{d}y \tag{46}$$

Inversion formula

$$\theta(x, y) = \sum_{n=1}^{\infty} K(\mu_n, y)\bar{\theta}(\mu_n, x) \tag{47}$$

The kernels $K(\mu_n, y)$ and the eigenvalues μ_n are those given by Eqs. (35) and (36), respectively.

Applying the operator $\int_0^{\gamma} K(\mu_n, y)\,\mathrm{d}y$ on Eq. (31) leads to the transformed form of the energy equation as

$$\frac{\partial^2\bar{\theta}(\mu_n, x)}{\partial x^2} - \mu_n^2\bar{\theta}(\mu_n, x) = C_n + C_n' \cosh \mu_n(2x-1)/2 \tag{48}$$

where

$$C_n = \left[-(-1)^n + 1\right]\sqrt{\frac{2}{\gamma}}\frac{1}{\mu_n} \times \left[\left(1+\frac{1}{\gamma}\right)^2\left(\hat{u}_s - \frac{P}{\mu_n^2}\right) - \frac{\hat{T}_s\mu_n^2}{1+\mu_n^2}\right] \tag{49}$$

$$C_n' = \left[-(-1)^n + 1\right]\sqrt{\frac{2}{\gamma^3}}\frac{P}{\mu_n^3\cosh \mu_n/2} \tag{50}$$

The boundary conditions at $x = 0$ and $x = 1$ are also transformed as

$$\bar{\theta}(\mu_n, 0) = \int_0^{\gamma} K(\mu_n, y)\theta(0, y)\,\mathrm{d}y = \sqrt{\frac{2}{\gamma}}\frac{\hat{T}_s[-(-1)^n + 1]}{\mu_n(1+\mu_n^2)} \tag{51}$$

$$\bar{\theta}(\mu_n, 1) = \int_0^{\gamma} K(\mu_n, y)\theta(1, y)\,\mathrm{d}y = \sqrt{\frac{2}{\gamma}}\frac{\hat{T}_s[-(-1)^n + 1]}{\mu_n(1+\mu_n^2)} \tag{52}$$

The transformed form of the energy equation, Eq. (48), is an ordinary differential equation the solution of which according to the boundary conditions, Eqs. (51) and (52), is

$$\bar{\theta}(\mu_n, x) = \frac{D_n \cosh \mu_n(2x-1)/2}{\cosh \mu_n/2} - \frac{C_n' \sinh \mu_n x}{4\mu_n \cosh \mu_n/2} + \frac{C_n' x \sinh \mu_n(2x-1)/2}{2\mu_n} - \frac{C_n}{\mu_n^2} \tag{53}$$

where

$$D_n = \left[-(-1)^n + 1\right]\sqrt{\frac{2}{\gamma^3}}\frac{1}{\mu_n^3}\left(\hat{u}_s - \frac{P}{\mu_n^2}\right) \tag{54}$$

Applying the inversion formula results in

$$\theta(x, y) = \sum_{n=1}^{\infty} K(\mu_n, y) \times \left[\frac{D_n \cosh \mu_n(2x-1)/2}{\cosh \mu_n/2} - \frac{C_n' \sinh \mu_n x}{4\mu_n \cosh \mu_n/2} + \frac{C_n' x \sinh \mu_n(2x-1)/2}{2\mu_n} - \frac{C_n}{\mu_n^2}\right] \tag{55}$$

Finally, the nondimensional temperature distribution is found by substituting Eqs. (27) and (55) into Eq. (21) as

$$\hat{T}(x, y) = \frac{\hat{T}_s}{1+e^{\gamma}}\left(e^{y} + e^{\gamma - y}\right) + \sum_{n=1}^{\infty} K(\mu_n, y) \times \left[\frac{D_n \cosh \mu_n(2x-1)/2}{\cosh \mu_n/2} - \frac{C_n' \sinh \mu_n x}{4\mu_n \cosh \mu_n/2} + \frac{C_n' x \sinh \mu_n(2x-1)/2}{2\mu_n} - \frac{C_n}{\mu_n^2}\right] \tag{56}$$

The only unknown, nondimensional slip temperature $\hat{T}_s$, may now be determined by nondimensionalizing Eq. (1), which gives the local nondimensional slip temperature at the bottom wall, and adapting to the other walls as

$$\hat{T}_s(x, 0) = \hat{T}_w + \frac{2\gamma\beta\beta_v Kn}{(1+\gamma)}\frac{\partial\hat{T}}{\partial y}\Big|_{y=0}$$

$$\hat{T}_s(x, \gamma) = \hat{T}_w - \frac{2\gamma\beta\beta_v Kn}{(1+\gamma)}\frac{\partial\hat{T}}{\partial y}\Big|_{y=\gamma}$$

$$\hat{T}_s(0, y) = \hat{T}_w + \frac{2\gamma\beta\beta_v Kn}{(1+\gamma)}\frac{\partial\hat{T}}{\partial x}\Big|_{x=0}$$

$$\hat{T}_s(1, y) = \hat{T}_w - \frac{2\gamma\beta\beta_v Kn}{(1+\gamma)}\frac{\partial\hat{T}}{\partial x}\Big|_{x=1} \tag{57}$$

where the parameter β is defined as

$$\beta = \frac{\beta_t}{\beta_v} \tag{58}$$

Integrating the local nondimensional slip temperatures along the walls, considering the uniform slip temperature and constant wall temperature (H1 boundary condition) along the walls, and averaging over the perimeter of microchannel give the average nondimensional slip temperature $\hat{T}_s$ as

$$\hat{T}_s = \left[\int_0^1 \hat{T}_s(x, 0)\,\mathrm{d}x + \int_0^1 \hat{T}_s(x, \gamma)\,\mathrm{d}x + \int_0^{\gamma} \hat{T}_s(0, y)\,\mathrm{d}y + \int_0^{\gamma} \hat{T}_s(1, y)\,\mathrm{d}y\right] \times \left[2(1+\gamma)\right]^{-1} \tag{59}$$

Since partial derivative of the temperature with respect y involves $\hat{T}_s$ term, the equation above is implicit in $\hat{T}_s$. Evaluating the integrals above and solving for the average nondimensional slip temperature result in its explicit form.

So far, the nondimensional velocity and temperature distributions are found, we may also determine the Nusselt number as

$$Nu = \frac{h D_h}{k} = \frac{q'}{(2a+2b)(T_w - T_b)} \frac{D_h}{k} = \frac{\gamma}{(1+\gamma)^2} \frac{1}{\widehat{T}_w - \widehat{T}_b} \tag{60}$$

where the bulk or average nondimensional temperature $\widehat{T}_b$ is defined as

$$\widehat{T}_b = \frac{1}{\gamma} \int_0^{\gamma} \int_0^1 \widehat{u}(x,y)\widehat{T}(x,y)\,\mathrm{d}x\,\mathrm{d}y \tag{61}$$

5. Results and discussion

The analysis above shows that the Nusselt number is a function of the wall temperature $\widehat{T}_w$, the aspect ratio γ, the parameter β and the rarefaction represented by $(\beta_v Kn)$. All the numerical calculations are done using "Mathematica 5" package with the wall temperature maintained at $\widehat{T}_w = 0$.

The aspect ratio γ varies from 1 (square microchannel) to zero (flat plate). The group $(\beta_v Kn)$, representing the rarefaction effect, ranges from 0.001 to 0.1 in slip flow. The parameter β is a function of the thermal accommodation coefficient F_t, the tangential momentum accommodation coefficient F_v, the specific heat ratio R and the Prandtl number Pr. For most of engineering applications both the F_v and F_t can be taken equal to unity, which lead to $\beta \cong 1.667$ for $R = 1.4$ and $Pr = 0.7$ [9]. Theoretically, β may vary from zero to high values such as 100. The particular case when $\beta = 0$ implies that the velocity slip at the solid boundaries is taken into account but the temperature jump is not.

The wall temperature dependence of the heat transfer in the microchannel is shown in Fig. 2. The constant Nusselt line ($Nu = 3.61$) in this figure corresponds to non-slip flow $\beta_v Kn = 0$, which does not show any variation with the wall temperature. As the rarefaction increases by increasing $(\beta_v Kn)$, the linear dependence of the Nusselt number on the wall temperature increases. Comparing the slop of the lines in Fig. 2 shows the increasing effect of the wall temperature on the Nusselt number with increasing rarefaction. However, the wall temperature dependence of the Nusselt number is very weak. Fig. 2 shows that going from zero nondimensional wall temperature to 1000, causes only a maximum %3.4 decrease in the Nusselt number. Therefore, the wall temperature dependence of the Nusselt number may be neglected in microchannel heat transfer under slip flow and H1 boundary condition.

Fig. 3 shows the rarefaction effect on the Nusselt number for β equal to 1.667, which is a characteristic value for most of engineering microchannel applications. A decrease in heat transfer with increasing rarefaction is investigated for

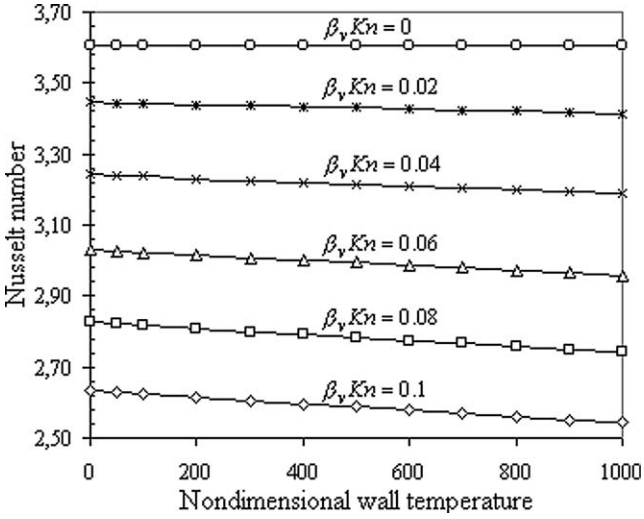

Fig. 2. Variation of the Nusselt number with wall temperature.

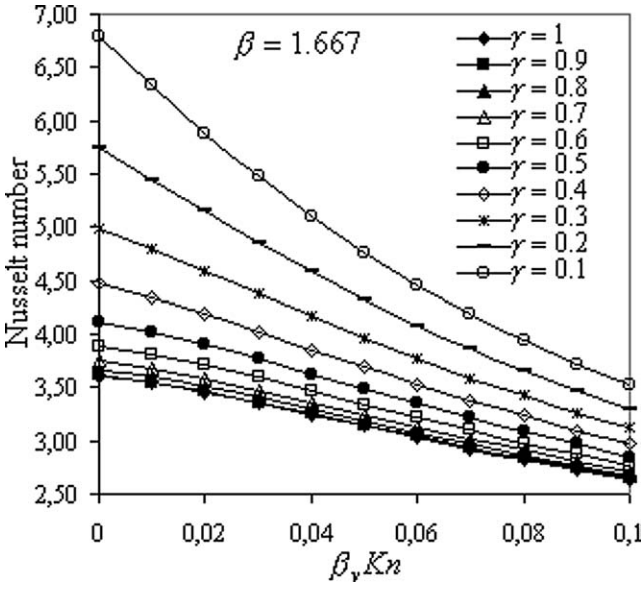

Fig. 3. Effect of the rarefaction on the Nusselt number for $\beta = 1.667$.

any aspect ratio. The decrease for low aspect ratios is sharper than that for high aspect ratios. The effect of microchannel size on the heat transfer can be well seen in Fig. 4. The figure shows that the heat transfer decreases with increasing aspect ratio. However, the rate of decrease slows down for aspect ratios higher than 0.5, specially at high rarefactions.

Fig. 5 shows the rarefaction effect on the Nusselt number when the temperature jump on the solid boundaries is not considered ($\beta = 0$). Excluding the temperature jump on the solid boundaries results in an increase in the heat transfer with increasing rarefaction for any microchannel size. Increasing rarefaction causes an increase in slip velocity on the boundaries that in turn causes an increase in heat transfer in the absence of temperature jump. As the temperature jump on the solid boundaries becomes slightly effective (low values of β), the rate of increase in heat transfer with rarefaction

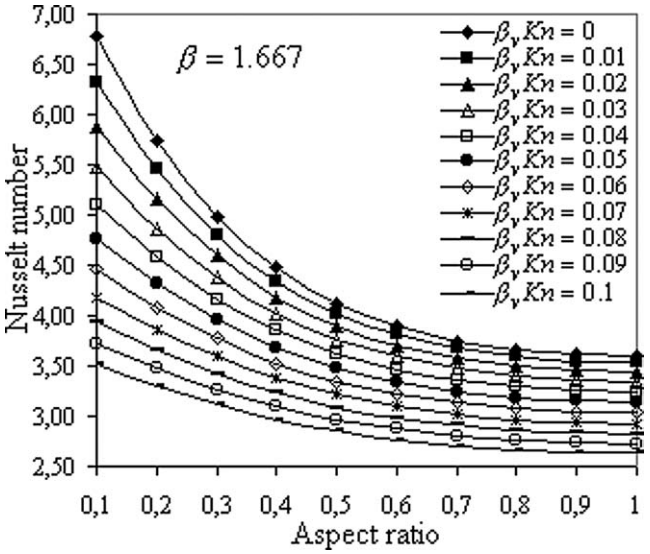

Fig. 4. Effect of the aspect ratio on the Nusselt number for $\beta = 1.667$.

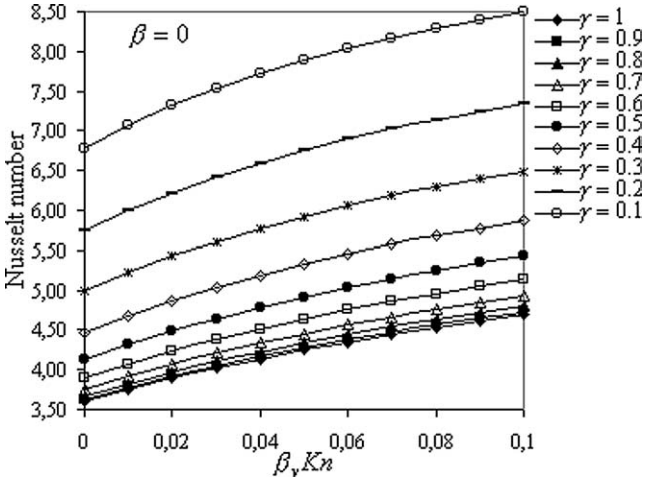

Fig. 5. Effect of the rarefaction on the Nusselt number for $\beta = 0$.

slows down. Fig. 6 shows this effect for a relatively low influence of temperature jump ($\beta = 0.5$). At high values of β a rapid decrease in heat transfer with rarefaction is expected. Fig. 7 investigates such an effect for $\beta = 10$.

The cumulative influence of temperature jump on the heat transfer can be seen in Fig. 8, which shows the variation of Nusselt number with β for a microchannel with $\gamma = 0.5$. The straight line on the top of figure ($Nu = 4.12$) corresponds to the case when both the velocity slip and temperature jump on the solid boundaries are absent (non-slip flow). The heat transfer, in general, decreases with increasing effect of the temperature jump (increasing β). However, the figure shows that for $\beta < 0.5$ the heat transfer increases and, for $\beta > 0.5$ the heat transfer decreases with rarefaction.

Setting $\beta_v Kn = 0$ in the calculations recovers the classical non-slip flow in ducts. The numerical values found for the Nusselt number with $\beta_v Kn = 0$ agrees exactly with those found by Morini [13] who solved the non-slip flow

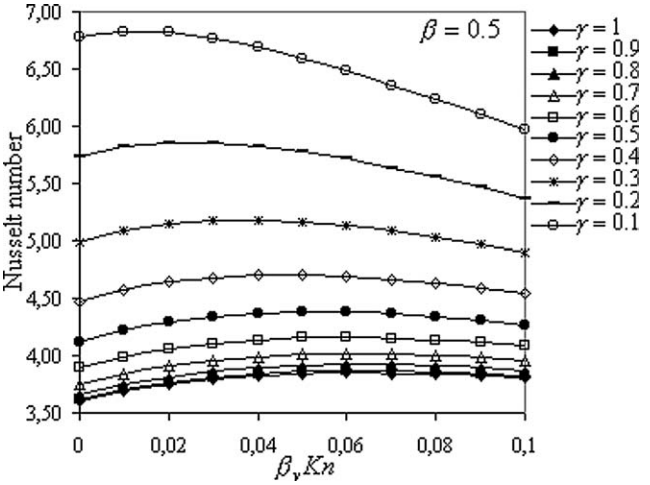

Fig. 6. Effect of the rarefaction on the Nusselt number for $\beta = 0.5$.

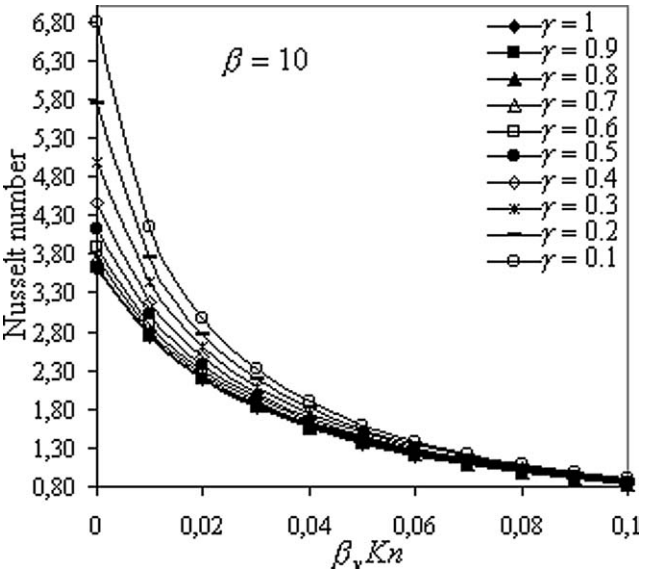

Fig. 7. Effect of the rarefaction on the Nusselt number for $\beta = 10$.

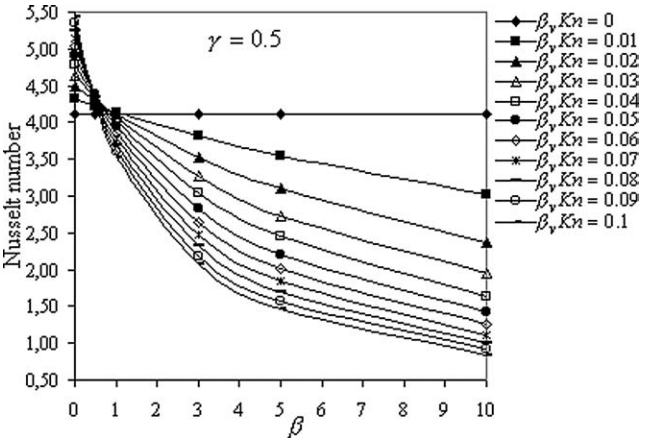

Fig. 8. Variation of the Nusselt number with β for a microchannel with $\gamma = 0.5$.

in ducts under H1 boundary condition. On the other hand, the numerical values of Nusselt number found in this paper are in good agreement with the numerical values of the "developed" Nusselt number found by Yu and Ameel [9]. Finally, it should be noted that the numerical calculations in this paper benefits of the fast convergence of the series that appear in the velocity and temperature distributions in microchannel. Compared with the works leading to a double infinite series, the present solution is advantageous in terms of calculation time due to the relatively simpler algebraic form of the series and appearing of a single infinite series.

Acknowledgements

The authors express deep appreciation to the reviewers for their constructive comments, suggestions and criticisms that improved the presentation of this paper.

References

[1] R.F. Barron, X. Wang, T.A. Ameel, R.O. Warrington, The Graetz problem extended to slip-flow, Internat. J. Heat Mass Transfer 40 (8) (1997) 1817–1823.
[2] T.A. Ameel, R.F. Barron, X. Wang, R.O. Warrington, Laminar forced convection in a circular tube with constant heat flux and slip flow, Microscale Thermophys. Engrg. 1 (4) (1997) 303–320.
[3] R.F. Barron, X. Wang, R.O. Warrington, T. Ameel, Evaluation of the eigenvalues for the Graetz problem in slip-flow, Internat. Commun. Heat Mass Transfer 23 (4) (1996) 563–574.
[4] F.E. Larrode, C. Housiadas, Y. Drossinos, Slip-flow heat transfer in circular tubes, Internat. J. Heat Mass Transfer 43 (15) (2000) 2669–2680.
[5] H. Zhao, The numerical solution of gaseous slip flows in microtubes, Internat. Commun. Heat Mass Transfer 28 (4) (2001) 585–594.
[6] M. Vasudeviah, K. Balamurugan, Stokes slip flow in a corrugated pipe, Internat. J. Engrg. Sci. 37 (12) (1999) 1629–1641.
[7] R.F. Barron, X. Wang, T.A. Ameel, R.O. Warrington, The Graetz problem extended to slip-flow, Internat. J. Heat Mass Transfer 40 (8) (1997) 1817–1823.
[8] Y.-P. Shih, C.-C. Huang, S.-Y. Tsay, Extended Leveque solution for laminar heat transfer to power-law fluids in pipes with wall slip, Internat. J. Heat Mass Transfer 38 (3) (1995) 403–408.
[9] S. Yu, T.A. Ameel, Slip-flow heat transfer in rectangular microchannels, Internat. J. Heat Mass Transfer 44 (22) (2001) 4225–4234.
[10] H.P. Kavehpour, M. Faghri, Y. Asako, Effects of compressibility and rarefaction on gaseous flows in microchannels, Numer. Heat Transfer A 32 (1997) 677–696.
[11] M. Vasudeviah, K. Balamurugan, Heat transfer of rarefied gases in a corrugated microchannel, Internat. J. Thermal Sci. 40 (5) (2001) 454–468.
[12] G. Tunc, Y. Bayazitoglu, Heat transfer in rectangular microchannels, Internat. J. Heat Mass Transfer 45 (4) (2002) 765–773.
[13] G.L. Morini, Analytical determination of the temperature distribution and Nusselt numbers in rectangular ducts with constant axial heat flux, Internat. J. Heat Mass Transfer 43 (5) (2000) 741–755.
[14] A. Beskok, G.E. Karniadakis, Simulation of slip-flows in complex micro-geometries, in: Micromechanical Systems. Book No. G00783-1992, in: ASME DSC, vol. 40, 1992, pp. 355–370.
[15] M. Gad-el-Hak, The MEMS Handbook, CRC Press LLC, Boca Raton, FL, 2002.